

1 Improving the particle dry deposition scheme in the CMAQ 2 photochemical modeling system

3 Qian Shu¹, Benjamin Murphy¹, Donna Schwede¹, Barron H. Henderson², Havala O.T. Pye¹, K.
4 Wyatt Appel¹, Tanvir R. Khan^{3*} and Judith A. Perlinger³

5 ¹ The Center for Environmental Measurement and Modeling, U.S. Environmental Protection Agency, Research
6 Triangle Park, NC 27711, USA.

7 ² Office of Air Quality Planning and Standards, U.S. Environmental Protection Agency, Research Triangle Park,
8 NC, 27711, USA.

9 ³ Department of Civil and Environmental Engineering, Michigan Technological University, Houghton, MI 49931,
10 USA.

11 * now with: FSEC Energy Research Center, University of Central Florida, Cocoa, 32922, USA.

12 *Correspondence to:* Qian Shu (shumarkq@gmail.com) and Benjamin Murphy (murphy.benjamin@epa.gov)

13 **Abstract.**

14 Dry deposition of atmospheric aerosols in large-scale models is a critical, but highly uncertain, sink process
15 with a strong dependence on particle size, meteorological conditions, and land surface properties. This study
16 investigates the particle dry deposition scheme implemented in the standard Community Multiscale Air Quality
17 (CMAQ) model v5.2.1, characterizes its underlying parameterized components with comparison to a similar scheme
18 in a contemporary regional-scale model, and proposes two updated schemes that are then evaluated with available
19 ambient particle deposition velocity (V_d) measurements. Both updated schemes reduce the surprisingly strong
20 dependence of deposition velocity on the aerosol mode width, with one scheme further introducing a dependence on
21 vegetation coverage that is broadly consistent with variability in observations between vegetated and non-vegetated
22 surfaces. Compared to the base scheme, the updated scheme with vegetation dependence increases V_d for submicron
23 particles and decreases it for larger particles by an average of 37% and -66%, respectively. This scheme performs
24 statistically better than the base scheme, reducing fractional biases by 56%-97% for vegetated land-use types and
25 has roughly equivalent performance over water. The base and updated schemes are tested with three annual CMAQ
26 (v5.2.1) simulations for the year 2011; predicted ambient aerosol concentrations are evaluated with routine
27 monitoring network observations and predicted dry deposition fluxes are evaluated with data from the Clean Air
28 Status and Trends Network (CASTNET). The updated scheme with vegetation dependence reduces negative
29 fractional biases for PM_{10} by 41% and positive fractional biases for $PM_{2.5}$ organic carbon by 15%. This scheme has
30 been incorporated into the most recent publicly accessible versions of CMAQ (v5.3 and beyond) to replace the
31 scheme used in previous versions of CMAQ (v4.5 through v5.2.1).

32 **1 Introduction**

33 Dry deposition is an essential removal process for atmospheric particles, which can account for more than
34 half of the total deposition of important chemical compounds in the atmosphere (Lovett, 1994). The ability of
35 atmospheric models to represent dry deposition processes directly affects the skill with which they can predict

36 particle concentrations, with implications for predictions of radiative forcing and the role of particles in climate
37 change (Emerson et al., 2020).

38 Several mechanistic or semi-empirical dry deposition schemes have been developed for scientific research
39 and operational purposes (Slinn et al., 1982; Ruijrok et al., 1995; Zhang et al., 2001, Petroff et al., 2008; Pleim and
40 Ran 2011; Saylor et al., 2019; Emerson et al., 2020), and implementation in chemical transport models (CTMs) is
41 challenging for several reasons. Khan and Perlinger (2017) evaluated five particle dry deposition parameterizations
42 from simple formulations to more complex and estimated 2-3 orders of magnitude uncertainty in V_d over a given
43 surface type and consistent ambient conditions, thus demonstrating that the functional form of the parameterization
44 can introduce significant variability for predicting V_d . An additional challenge to interpreting the potential impact of
45 the choice of particle deposition schemes is that until recently, measurement studies often reported the deposition
46 flux for bulk particles at one or two nominal sizes, making it difficult to evaluate V_d across the particle size
47 distribution. Previous reviews (Pryor et al., 2008 and Petroff et al., 2008) have pointed out the value in unified
48 studies that combine numerous measurements and modeling methods. Finally, as Zhang (2001) noted when
49 investigating several schemes for calculating V_d as a function of particle size, some schemes have limited
50 applicability beyond one land-use type (Slinn and Slinn, 1980; Davidson et al., 1982; Wiman and Ågren, 1985;
51 Peters and Eiden, 1992) while others apply to multiple types (Schemel and Hodgson, 1980; Haynie, 1986; Giorgi,
52 1988). The variability among these studies emphasize the importance of using measurements to assess and improve
53 process-based dry deposition schemes across diverse land-use types (e.g. vegetated, water, desert and snow), even
54 though existing measurements are limited to a few specific types (Nemitz et al., 2002). Newly revised semi-
55 empirical particle dry deposition schemes by Saylor et al. (2019) and Emerson et al. (2020) successfully describe
56 observations across a variety of land-use types. Nevertheless, it can be difficult to apply and interpret the impact of
57 sophisticated schemes for use in CTMs, which vary in their representation of atmospheric particles.

58 When CTMs use higher accuracy, process-based dry deposition schemes, physical properties of particles
59 are needed from the host CTM. These models represent particle distributions using a number of possible approaches
60 including 1) modal methods, which employ particle modes with a median particle size and standard deviation (e.g.,
61 the Community Multiscale Air Quality (CMAQ) model, Binkowski and Shankar (1995)), 2) bulk methods, which
62 rely on a single particle size (e.g., the Comprehensive Air Quality Model with extensions (CAMx) coarse-fine
63 option), and 3) sectional bin methods, which apply a series of discrete size bins (e.g., GEOS-Chem Two-Moment
64 Aerosol Sectional model, Emerson et al. (2020); CAMx Carnegie Mellon sectional aerosol option). Saylor et al.
65 (2019) compared several existing schemes with a newly developed empirical sectional scheme and determined that
66 fine-particle concentration predictions at the surface may vary by 5%-15% depending on the choice of particle V_d
67 scheme. A previous study from Shu et al. (2017) determined that particle dry deposition scheme differences between
68 two regional CTMs, CMAQv5.0.1, and CAMx v5.4.1, drove differences in predicted organic aerosol (OA)
69 concentrations when controlling for differences in emissions, meteorology, and chemistry in both models. Although
70 that study did not evaluate the performance of each model's particle dry deposition scheme specifically, it pointed
71 out that constraining the magnitude of this loss process may be as important as predicting the magnitude of
72 production of atmospheric pollutants from key anthropogenic and biogenic sources.

73 In the present study, we explore the source of discrepancies between CMAQ and CAMx particle dry
74 deposition results documented by Shu et al. (2017) by comparing schemes from both models within an offline box
75 model framework for monodisperse particle populations of varying sizes and across land-use types. This box model
76 calculates particle dry deposition velocity under specific environmental conditions. We then propose incremental
77 revisions to the CMAQ scheme and characterize behavior of these updates in the box model with specific focus on
78 demonstrating the impact of integrating across polydisperse particle modes. Finally, we implement each proposed
79 CMAQ scheme into the full CMAQv5.3 model platform (released August 2019), and evaluate performance across
80 land-use types using available field measurements to verify the accuracy of each selected scheme. Finally, we
81 document the impact that the dry deposition scheme revisions have on CMAQ-predicted ambient aerosol
82 concentration for an entire simulation year.

83 2 Methods

84 2.1 Particle dry deposition schemes in CMAQ and CAMx

85 Particle dry deposition is a complex process that depends on the chemical and physical properties of
86 particles, which are related to their source and composition, as well as the features of the underlying land surface
87 and the proximate meteorological conditions. Typically, the flux of particle mass through the surface boundary layer
88 is mathematically expressed as (Wesely and Hicks, 1977)

$$89 F(z) = C(z)V_d, \quad (1)$$

90 where $F(z)$ is the vertical flux of a pollutant in the surface boundary layer, $C(z)$ is the concentration at a specific
91 height in the surface layer, and V_d is the deposition velocity.

92 The CMAQ model has used the dry deposition scheme of Pleim and Ran (2011), referred to as PR11, for
93 model versions v4.5 through v5.2.1. The scheme is based on the Slinn (1982) approach and introduces various
94 modifications. The dry V_d , derived by Venkatram and Pleim (1999), is a function of the settling velocity (V_g), the
95 aerodynamic resistance (R_a), and the surface layer resistance (R_s ; called the quasi-laminar sub-layer resistance by
96 Pleim and Ran(2011)) as shown in Table 1 and discussed in section S1. The aerodynamic resistance is defined by
97 Pleim and Ran (2011) to be equal to the Slinn (1982) definition scaled by a non-dimensional temperature profile
98 constant under neutral conditions. As shown in Table 1, R_s is inversely dependent on the product of the sum of
99 Brownian and impaction efficiencies, the friction velocity (u_*), and an empirical correction factor (F_f) to account for
100 increased deposition in convective conditions as suggested by Wesely et al (1985).

101 Formulations for the collection efficiency term components are shown in Table 2. For example, efficiency
102 due to Brownian diffusion (E_B) was parameterized in Slinn (1982) as $E_B = Sc^{-\frac{2}{3}}$ where the Schmidt number (Sc) is
103 defined in section S1 (Eq. S8). The exponent of this form is typically assumed to range between 1/2 for smooth
104 surfaces and 2/3 for rough surfaces. Pleim and Ran (2011) adopted the recommendations of Slinn (1982) and Giorgi
105 (1986) to represent the impaction efficiency E_{IM} as $\frac{St^2}{400+St^2}$. This formulation has a weaker dependence on the Stokes
106 number relative to other forms proposed by Slinn (1982) and was fit to data from Liu and Agarwal (1974) by Giorgi

107 (1986). For the interception collection efficiency (E_{IN}), a process characterized by uptake onto small collectors in
 108 the canopy, Pleim and Ran (2011) acknowledged that Slinn (1982) proposed an expression that may be important
 109 for vegetative surfaces but neglected it in the CMAQ model parameterization because the CMAQ M3DRY dry
 110 deposition module (the only option available for dry deposition prior to v5.3) uses grid-averaged values of the
 111 surface parameters, making it difficult to specify realistic estimates of parameters like characteristic leaf size in a
 112 grid-scale model. The interception process has been shown by Emerson et al. (2020) to be potentially critical for
 113 capturing the deposition velocity of fine particles, although the authors note that it has the least physical basis of the
 114 deposition processes considered and is highly dependent on parameterization and optimization with ambient
 115 observations.

116 The PR11 scheme is applied in CMAQ by integrating the particle size-dependent parameters across each
 117 particle mode using the geometric mean diameter and standard deviation (Binkowski and Shankar, 1996). The
 118 integrated settling velocity (\widehat{V}_g) and integrated Brownian diffusivity (\widehat{D}) that is needed for the calculation of the Sc
 119 (Eq. S8) are defined as:

$$121 \widehat{V}_{g,k} = V_g \left\{ \exp\left(\frac{4k+4}{2} \ln^2 \sigma_g\right) + 1.246Kn_g \exp\left(\frac{2k+1}{2} \ln^2 \sigma_g\right) \right\} \quad (2)$$

$$123 \widehat{D}_k = D \left\{ \exp\left(\frac{-2k+1}{2} \ln^2 \sigma_g\right) + 1.246Kn_g \exp\left(\frac{-4k+4}{2} \ln^2 \sigma_g\right) \right\} \quad (3)$$

124
 125 where k is the moment of the size distribution being considered, σ_g is the standard deviation of an aerosol mode, and
 126 Kn is the Knudsen number calculated with the modal geometric mean diameter. CMAQ uses three moments to
 127 describe the particle population: the zeroth (equal to number concentration), second (proportional to surface area
 128 concentration), and third (proportional to volume and mass concentration). Instead of using the modal-integrated
 129 settling velocity for calculation of the Stokes number in the impaction efficiency formulation, Pleim and Ran (2011)
 130 integrated the impaction efficiency \widehat{E}_{IM} directly as shown in Table 3. They also simplified the denominator of the
 131 impaction efficiency from its form in Table 2 to facilitate integration of the impaction efficiency, similar to the other
 132 modal-integrated terms, although the rationale for, and impact of, this choice was not documented. This form of \widehat{E}_{IM}
 133 is then applied to calculate R_s in CMAQ but can lead to exceedingly large V_d for σ_g greater than 2 (section S1.2).

134 The CAMx model uses the scheme of Zhang et al. (2001), hereafter referred to as Z01, with V_d defined in
 135 Table 1. The Z01 scheme's collection efficiency parameters and dependencies are detailed in Table 2 and supporting
 136 section S2. Crucially, the CAMx coarse-fine implementation, which was analyzed in Shu et al. (2017) and will be
 137 the focus here, does not consider of polydispersity of the particle population. On the contrary, all fine and coarse
 138 particles are assumed to have a diameter of approximately 1 and 5 μm , respectively. The major differences between
 139 Z01 and PR11 are 1) the modal integration of diffusivity, settling velocity, and impaction efficiency in the PR11
 140 scheme, 2) the use of interception efficiency in the Z01 scheme for vegetative surfaces, 3) the formulation of the
 141 impaction efficiency in the Z01 scheme, which includes a coefficient (α) that varies with land-use type rather than
 142 being fixed as in the PR11 scheme, and 4) the dependence of R_s on the convective velocity scale (w_*) in the PR11

143 scheme. For this study, we focus specifically on the differences introduced between the schemes by modal
144 integration and dependence on vegetation coverage.

145 Rather than comparing output from the full CAMx and CMAQ models, we have developed a convenient
146 and unified zero-dimensional box model (DepoBoxToolv1.0; see section S3) with which we predict V_d for the Z01
147 and PR11 schemes for four land-use types (e.g., grass, coniferous forest, deciduous forest and water) using inputs
148 describing the monodisperse particle sizes and meteorological conditions (Table S1).

149 **2.2 Proposed updates to CMAQ scheme**

150 We explore two incremental revisions to the existing PR11 scheme to facilitate better representation of
151 integration of deposition across aerosol sizes and dependence on ground vegetation. The first revised scheme, OFF,
152 is designed to stabilize the influence of σ_g on E_{IM} . This scheme removes the explicit integration of E_{IM} (Table 3),
153 and instead uses the monodisperse forms of the Stokes number and original formulation of E_{IM} from Giorgi (1986)
154 and reported by Pleim and Ran (2011). To restore size dependence to E_{IM} , a second revised scheme, VGLAI, uses
155 the integrated form of gravitational settling velocity in the calculation of the Stokes number (Table 3). Additionally,
156 this revised scheme adjusts the constant in the E_{IM} expression denominator to 1.0, which is more suitable for
157 vegetation (Zhang et al., 2001) and adds dependencies on leaf area index (LAI) and the grid cell vegetation-coverage
158 fraction (f_{veg}) to the surface resistance expression (Table 1). The desired role of this empirical correction factor is to
159 increase the influence of collection on vegetative surfaces, especially for small particles. As intended, the surface
160 resistance (R_s) decreases with both increasing LAI and f_{veg} and is most important for particles with diameter less
161 than 1 μm . When LAI goes to 1 or f_{veg} goes to 0 (i.e., smooth surfaces), dry deposition velocity converges to that of
162 the OFF scheme (Fig. S3).

163 To assess the reasonableness of the PR11, OFF and VGLAI schemes, we have gathered available field data
164 for measured particle dry V_d (Table S2) as a function of particle size across land-use types (e.g., grass, coniferous
165 forest, deciduous forest and water). We again employ the zero-dimensional DepoBoxToolv1.0 with which we
166 predict V_d for the schemes discussed here using inputs describing the particle population and meteorological
167 conditions coincident with each observation (Table S1). Although published field data provide measured V_d and
168 corresponding particle size, the descriptions of environmental parameters are less consistently documented. In many
169 cases, meteorological or surface input parameters are missing from datasets and must be approximated for
170 DepoBoxToolv1.0 calculations. We evaluate the schemes for all four different land-use types and vary parameters
171 for the modeled aerosol size distribution (i.e., geometric mean diameter and modal standard deviation) to quantify
172 the sensitivity of each scheme's performance to these two critical model inputs.

173 **2.3 CMAQ simulation and evaluation**

174 We conducted three annual simulations during 2011 using CMAQv5.2.1, each using a different deposition
175 scheme (i.e., PR11, OFF, and VGLAI). The modeling domain is a 12 km x 12 km resolution grid covering the
176 conterminous U.S. and extending to 50 hPa in altitude with 35 vertical layers and higher resolution near the Earth's
177 surface. The lowest model layer is approximately 20 meters deep. Emissions for 2011 are tabulated from

178 information provided by states and other federal agencies via the 2011 National Emissions Inventory (NEI;
179 <https://www.epa.gov/>). The emissions estimates were further allocated temporally to hourly resolution for the entire
180 year 2011 and in spatially to each grid cell in the 12 km x 12 km model domain by the Sparse Matrix Operator
181 Kernel Emissions (SMOKE; <https://www.cmascenter.org/smoke/>) program. Plume rise for elevated point sources
182 was calculated online in CMAQ, as were NO_x emissions from lightning strikes (Kang et al., 2019). Biogenic
183 emissions of volatile organic compounds were predicted online with the Biogenic Emission Inventory System (Bash
184 et al., 2016) and offline meteorology was calculated with the Weather Research and Forecasting (WRF) model
185 version 3.7. Chemical boundary conditions for the model were driven by a hemispheric application of the GEOS-
186 Chem model (Henderson et al., 2014) simulation for 2011 (Appel et al., 2017). Four-dimensional data assimilation
187 (FDDA) was employed. Wind-blown dust emissions were calculated as documented by Foroutan et al. (2017).
188 Specific land cover information was obtained from the National Land Cover Database (NLCD;
189 <https://www.usgs.gov/centers/eros/science/national-land-cover-database>) and LAI information was gathered from
190 satellite products from the MODIS (<https://modis.gsfc.nasa.gov>) satellite. CMAQv5.3 has two options for modeling
191 atmosphere-surface exchange of gases and particles. The M3DRY dry deposition module was used for the analysis
192 by Shu et al. (2017), while the Surface-Tiled Aerosol Gas Exchange (STAGE) module (available in CMAQv5.3)
193 provides a detailed, land-use specific framework for representing pollutant fluxes to and from various land-use types
194 contributing to each model grid cell (Appel et al., 2020). Because this study is primarily concerned with the impact
195 of the particle deposition scheme when comparing historical and modern CMAQ versions, we narrow our focus to
196 just simulations with the M3DRY module.

197 Outputs for ambient concentration and dry deposition flux from the three CMAQ simulations are paired in
198 space and time with observed data using the atmospheric model evaluation tool (AMET, Appel et al., 2011). There
199 are several regional and national networks that provide routine observations of particle species in the U.S. for
200 CMAQ evaluation. In this study, we use measurement data sets from the Interagency Monitoring of Protected Visual
201 Environments (IMPROVE, 157 sites; <http://vista.cira.colostate.edu/improve/>), Chemical Speciation Network
202 (CSN; 171 sites; <https://www3.epa.gov/ttnamti1/speciepg.html>), the EPA Clean Air Status and Trends Network
203 (CASTNET, 81 sites; <https://www.epa.gov/castnet>) and the EPA Air Quality System (AQS, 4000+ sites;
204 <https://www.epa.gov/aqs>). As a database for various networks, AQS data also contain the same data that are in CSN,
205 IMPROVE, and CASTNET.

206 Nolte et al. (2015) investigated fine and coarse mode size distribution performance for CMAQv5.0,
207 finding that many sites and chemical species contributions were well-reproduced, but the model tended to
208 underpredict concentrations of large particles in sites dominated by soil dust. Appel et al. (2020) showed that
209 CMAQv5.3 demonstrates impressive model skill predicting ambient fine PM concentrations when compared with
210 routine measurement networks, including CSN and IMPROVE network. Statistical analysis of concentration, bias,
211 root mean square error (RMSE) and the Pearson correlation coefficient of monthly average bulk PM_{2.5} for 2016
212 between standard CMAQv5.2.1 (PR11) and CMAQv5.3.1 (with VGLAI incorporated) also showed that results of
213 CMAQv5.3.1 are improved compared to CMAQv5.2.1.

214 3. Results and Discussion

215 3.1 Characterization of existing CMAQ and CAMx dry deposition schemes

216 To better understand the impact of each particle dry deposition scheme on predictions in the CMAQ and
217 CAMx models, we visualize their size-dependence across four land-use types (grass, coniferous forest, deciduous
218 forest, and water) in Fig. 1. For the PR11 scheme, the trends are integrated to estimate the deposition of the third
219 moment of the modal particle size distribution, which is applied to calculate the loss of particle mass in CMAQ. The
220 x-axis corresponds to the geometric mean diameter for the PR11 trends. For the Z01 scheme, the trend shown is for
221 monodisperse particles, consistent with the application of the scheme to calculate particle mass loss in the CAMx
222 model. Figure 1 demonstrates the large impact of σ_g on the value of V_d in the PR11 scheme. When σ_g equals 1.01 (i.e.
223 monodisperse particle population), PR11 predicts roughly similar V_d as Z01 for sizes above 5 μm over grass and
224 water surfaces. However, PR11(1.01) deviates from Z01 for sizes under 5 μm across all land-use types and to some
225 degree for sizes above 5 μm over forest surfaces. The greatest discrepancies between schemes occur over coniferous
226 (and to a lesser degree deciduous) forests where the PR11(1.01) V_d increases more steeply for coarse particles than
227 the Z01 scheme due to the larger magnitude of the impaction efficiency. At smaller particle sizes ($d_p < 1 \mu\text{m}$),
228 PR11(1.01) V_d is smaller than that of Z01 by a factor of 5-10, and this difference diminishes with decreasing particle
229 size. For the vegetative land-use types, the deviation at small particle sizes is mostly explained by the interception
230 efficiency used in the Z01 scheme (Table 2) since the different formulations for V_d lead to at most a 30% difference
231 between the two schemes (Fig. S1). Impaction is likely not playing a large role for particles in the submicron regime
232 (see for example, Emerson et al., 2020). The schemes are roughly equivalent for water surfaces where the forms of
233 Brownian, impaction, and interception efficiency are most similar. Saylor et al. (2019) compared the PR11 scheme
234 with varying w^* to the Z01 scheme for broadleaf, needleleaf, cropland, and urban land-use types and found similar
235 results to those reported here for the $\sigma_g = 1.01$ case (see also Fig. S4).

236 Despite general similarity between the PR11(1.01) and Z01 schemes, PR11 estimates of V_d change
237 dramatically when modal integration is considered. As σ_g increases, the PR11(1.7) and PR11(2.5) predictions for
238 third moment V_d increase rapidly with increasing particle size across all land-use types (e.g., factors of 49 and 70,
239 respectively, larger than Z01 at $d_p = 1 \mu\text{m}$). This is consistent with the large differences found between CMAQ and
240 CAMx for fine-mode mass V_d by Shu et al. (2017). When σ_g increases from 1.01 to 2.5, it is expected to reflect this
241 characteristic shift of the V_d trend to smaller particle sizes. Because the modal integration approach with larger σ_g is
242 influenced by larger particles ($d_p > 10 \text{ m}$) where V_d is orders of magnitude larger, PR11(1.7) and PR11(2.5) tend to
243 predict higher V_d at mid-range particle size ($0.2 < d_p < 1 \text{ m}$) relative to PR11(1.01). Meanwhile, at smaller sizes (d_p
244 $< 0.1 \text{ m}$), PR11(1.7) and PR11(2.5) predict lower V_d than PR11(1.01) since they are influenced by midsize particles
245 ($0.2 < d_p < 1 \text{ m}$) where V_d is orders of magnitude smaller. The minimum V_d for the PR11(2.5) scheme shifts
246 compared to PR11(1.01) from approximately 1.0 to 0.1 μm . Pleim and Ran (2011) found the same behavior when
247 introducing the formulation for the PR11 impaction efficiency but did not discuss its magnitude in the context of
248 particle dry deposition schemes in contemporary CTMs or other model deposition processes. Detailed inspection of
249 the sensitivity of the third moment V_d on σ_g , introduced by the formulation of the integrated impaction efficiency,
250 suggests that the PR11 scheme predicts unrealistically large V_d at large σ_g (section S1). Overall, our results indicate

251 that the discrepancy in particle dry deposition schemes documented by Shu et al. (2017) are partly driven by an
252 expected increase in V_d when properly considering the polydispersity of aerosol modes but are also exacerbated by
253 an unconstrained integration approach for the impaction efficiency.

254 3.2 Evaluation of CMAQ dry deposition schemes

255 Evaluation of the third moment V_d from the PR11 scheme and two revised schemes (OFF and VGLAI)
256 with field data demonstrates that the revised schemes have similar magnitude and size-dependence to the PR11
257 scheme (Fig. 2). When $\sigma_g = 1.01$, all schemes reflect monodisperse particle populations and OFF is equivalent to
258 PR11. However, the predicted V_d is sensitive to σ_g , shifting to the left as σ_g increases from 1.01 to 2.5. For water
259 surfaces, the schemes give nearly identical results across all ranges of d_p . While observed data over water surfaces is
260 sparser than that for land-based surfaces, the limited data available suggest that all three schemes are
261 underpredicting the deposition of coarse particles over water and are possibly overpredicting deposition of
262 submicron particles. For grass surfaces, VGLAI markedly increases V_d beyond that of both the PR11 and OFF
263 schemes in the sub-micron particle range. This feature is enhanced further for both forest types, characterized by
264 taller canopies and greater LAI than that for grass. All three schemes appear to miss the sharp increase in V_d starting
265 at ~ 100 nm particle diameters and thus underpredict the deposition of accumulation mode particles. Emerson et al.
266 (2020) showed that this trend could be approximated using a form of the Slinn (1982) model with an increased role
267 of particle interception efficiency determined from an empirical fit. Saylor et al. (2019) added an efficiency term for
268 an unknown process and empirically fit its value for discrete size ranges, which can be applied in a sectional aerosol
269 model. Graphically, the VGLAI scheme appears to perform incrementally better at capturing the observed
270 magnitude of V_d over vegetative surfaces than the PR11 and OFF schemes. Future work on CMAQ dry deposition
271 schemes will address the current discrepancy between schemes based on Pleim and Ran (2011) and relatively high
272 V_d for accumulation mode particles. As σ_g increases to 1.7, where all schemes represent relatively narrow
273 polydisperse particle populations, the PR11 overestimates V_d in the 2-10 μm range compared to available
274 observations for coniferous forest surfaces. The OFF and VGLAI schemes both reduce V_d in this range as revisions
275 of impaction efficiency integration take effect. All schemes still show the same performance on the water. When σ_g
276 increases to 2.5, the trends of the three schemes sharply shift to the left, significantly deviating from observed data
277 for coarse particles over grass and coniferous forests. All schemes seem to capture more observations in the 0.1-1
278 μm range over the two forest types, perhaps indicating a role for polydispersity in historical bulk particle
279 measurements.

280 Deposition velocity predicted by all schemes is statistically evaluated for $\sigma_g = 1.01$ to reflect monodisperse
281 particle populations (Table 4), consistent with other studies (e.g., Saylor et al., 2019). Our results show that all
282 schemes statistically underpredict V_d across particle sizes and land-use types, which is also consistent with Saylor et
283 al. (2019). Generally, these results show that the revisions incorporated in the VGLAI scheme better reproduce
284 ambient observations of V_d than the PR11 scheme, with negative fractional biases reduced by factors of 9.2, 37.7,
285 and 2.26 for grass, coniferous forest, and deciduous forest surfaces, respectively. The VGLAI also improves
286 fractional biases and errors when evaluated with alternative σ_g (1.7 and 2.5, see Table S3). Correlation coefficients

287 across all σ_g are similar or slightly smaller with the VGLAI scheme, a consequence of the PR11 scheme
288 approximating the shape of the V_d observation trend as in Fig 2. It is noted that correlation coefficients for
289 deciduous forest are quite lower than other land use types. This could be the imperfection of collected deciduous
290 datasets. Not all measurements have well stated their measured d_p or σ_g , thus assumptions were made. And some
291 studies reported abundant data while others only have sparse data points (Table S2). Generally, results suggest that
292 large values of σ_g significantly impact the polydisperse V_d and should be used cautiously in CMAQ. Nevertheless,
293 with an appropriate choice of σ_g (e.g., 1.01 or 1.7), the OFF and VGLAI schemes improve numerical stability over
294 the PR11 scheme for 1-10 μm particles where the impaction efficiency is important. Saylor et al. (2019) pointed out
295 that PR11 scheme was sensitive to the value of w_* , which can vary significantly as a function of the surface
296 roughness, defined for each land-use type. Even if explicit w_* can be acquired from WRF output when PR11 is
297 implemented in CMAQ, it is not practical to apply all explicit w_* in box model scale. Therefore, assumed w_* is used
298 for box scale evaluation as Saylor et al. (2019). The sensitivity of dry deposition schemes is tested in Fig. S4, and it
299 shows that the uncertainty introduced by the convective correction factor, F_f , is also important to consider for sub-
300 micron particles, particularly sub-300 nm particles for wider modes.

301 3.3 Impact on CMAQ particle dry deposition velocity

302 Although the box model characterization and evaluation results illuminate the process-level impacts of
303 revising the particle V_d algorithm, a broader analysis of dry V_d within the context of a regional-scale simulation is
304 needed to fully understand the impact that the OFF and VGLAI schemes have on CMAQ model performance and
305 deposition predictions. We first inspect the change in dry V_d summarized for the entire model domain for Aitken,
306 accumulation, and coarse mode particles.

307 From the box-whisker plots of annually averaged V_d shown in Fig. 3, OFF and VGLAI both reduce the
308 median V_d of coarse-mode particles by 79% and 72%, respectively, compared to the PR11 simulation. For Aitken-
309 mode particles, the revision in the OFF scheme has little impact on V_d compared to PR11 while using VGLAI
310 increases the median V_d by 47% while also increasing the 95th percentile from 0.29 to 0.56 cm s^{-1} . For accumulation
311 mode particles, OFF reduces median V_d by 24%, while the LAI correction to the VGLAI scheme increases median
312 V_d by 22%. The change in coarse-mode particle deposition velocity is similar across all major land-use types (Fig.
313 S5), including water. The slight increase in V_d for the coarse mode when revising the OFF scheme to VGLAI is a
314 result of integrating the settling velocity when calculating the impaction efficiency, as well as revising the form of
315 the impaction efficiency expression (Table 3). For vegetative land-use types, the Aitken-mode V_d changes resemble
316 that of the total domain-wide change, where PR11 and OFF have similar V_d distributions while the VGLAI scheme
317 increases V_d . For water surfaces, predictions with the three schemes have similar distributions of V_d for the Aitken
318 mode.

319 Figure 4 shows the spatial variation in annual mean third-moment dry V_d of the three particle modes
320 (Aitken, accumulation, coarse) for the PR11 scheme and the impact of the revised parameterizations on the PR11
321 dry V_d predictions. There generally exists orders of magnitude difference in V_d among different particle modes
322 consistent with box model results and established literature (Aitken: $V_d = 0.03\sim 0.55 \text{ cm s}^{-1}$, accumulation: $V_d =$

0.01~0.72 cm s⁻¹, coarse: $V_d = 0.43\sim 18.37$ cm s⁻¹). For a given aerosol mode, V_d varies considerably for different land-use types. But even when controlling for particle size and land-use type, the three CMAQ simulations have significant differences in V_d across the entire domain. Compared with PR11, OFF systematically reduces the V_d of coarse mode particles by an average of 65% over the entire domain. For the Aitken mode, OFF has less impact than it does for the coarse mode, reducing V_d by less than 8% across the model domain. Comparison of the accumulation mode, however, indicates a stronger downward adjustment in elevated regions of the Rocky and Appalachian Mountains (-61%) and less impact in the plains and low-lying areas of the southeast (-8%). VGLAI predicts similar V_d reductions to the OFF scheme for coarse particles but increases V_d by an average of 59% for the Aitken mode, particularly in the forests of the southeast US (up to 305%). For accumulation mode particles, VGLAI shows spatial diversity of V_d perturbations compared to PR11. This is because the LAI correction factor and impaction efficiency revisions are independently important for the Aitken and coarse modes, respectively, but they are both relevant for calculating the accumulation mode V_d . The impaction efficiency revision leads to a net decrease on average over the highest elevated mountainous regions where CMAQ predicts larger and broader than average accumulation modes, while the LAI dependence of the VGLAI scheme ensures net enhancements in V_d over the southeast, south, west coast, and central Canada where accumulation mode parameters are predicted to be smaller and narrower than average (i.e., close to sources).

Evaluation of predicted SO_4^{2-} , NO_3^- and NH_4^+ using CASTNET inferential deposition estimates, similar to Saylor et al. (2019), are summarized in Table 5. Compared to PR11, VGLAI reduces negative fractional biases of SO_4^{2-} , NO_3^- deposition by 18.8% and 11.7% and positive biases of NH_4^+ deposition by 15.3%. Fractional errors decrease as well for SO_4^{2-} and NO_3^- but increase for NH_4^+ . As Saylor et al. (2019) argued, these inferred dry deposition observations are not ideal for evaluating a regional-scale photochemical grid model like CMAQ, but they offer additional evidence that the VGLAI scheme is performing reasonably.

3.4 Impact on CMAQ ambient particle concentrations

Histograms of the change in annual mean concentration predicted by CMAQ for aggregate PM mass metrics using the OFF and VGLAI schemes is shown in Fig. 5. The histograms depict spatial variability in annual mean values over the CMAQ domain. The OFF scheme predicts greater concentrations of all aggregate PM for PM_{10} , PM coarse (PMC; $2.5 < d_p < 10$ μm), $\text{PM}_{2.5}$, $\text{PM}_{2.5}$ organic matter (OM), and $\text{PM}_{1.0}$, respectively. Meanwhile, the VGLAI impact is larger for smaller particles, with reductions for $\text{PM}_{1.0}$ and $\text{PM}_{2.5}$ OM concentrations by as much as -0.78 and -0.47 $\mu\text{g m}^{-3}$, respectively. The concentration change distributions for these metrics are characterized by long tails, and most grid cells change by less than -0.2 $\mu\text{g m}^{-3}$. For $\text{PM}_{2.5}$, VGLAI concentration changes range from -0.7 to 0.8 $\mu\text{g m}^{-3}$ depending on location. The histograms for PM_{10} and $\text{PM}_{2.5}$ are also plotted by land-use categories in Fig. S6 and S7 based on the map of dominant land use (Fig. S10). Because of their elevated importance as criteria air pollutants, we show the annual mean surface concentrations of PM_{10} and $\text{PM}_{2.5}$ simulated by PR11 in Fig. 6, along with the relative percent changes when the OFF and VGLAI schemes are used. Similar maps of $\text{PM}_{2.5}$ chemical components (NO_3^- , NH_4^+ , SO_4^{2-} , element carbon (EC), and OM) are provided in Fig. S8 as well as PM_{10} (Fig. S9). As CMAQ does not treat EC and OM in coarse mode, only NO_3^- , NH_4^+ , SO_4^{2-} are plotted for PM_{10} .

359 CMAQ simulations using the OFF and VGLAI schemes predict much higher PM_{10} concentrations over the western
360 US, ranging from +4.3 % to +122 %, a result of substantially lower predicted V_d for the coarse mode particles (Fig.
361 4D, G). For $PM_{2.5}$, the updated schemes predict more modest changes (-5.8% to 19.3%). This is due to the
362 diminishing influence of the impaction term in the PR11 scheme on decreasing particle size. The OFF scheme
363 introduces essentially no change to the aerosol concentrations over vegetative areas in the eastern U.S. but does
364 result in a significant increase in concentrations in the southwest U.S. With the VGLAI scheme in place,
365 concentrations decrease modestly (less than 10%) in regions outside the southwest U.S.

366 This modest impact on $PM_{2.5}$ concentrations is broadly consistent with the depiction of accumulation mode
367 V_d in Fig. 4F, as the predicted magnitude of V_d for the accumulation mode is quite small in the PR11 scheme.
368 However, the impact on speciated components is more complex (Fig. S8). Annual-averaged concentrations of bulk
369 $PM_{2.5}$ increase slightly with the OFF scheme, driven mainly by enhancements in OM, SO_4^{2-} , and to a lesser extent,
370 EC. Ammonium concentrations decrease throughout the US, and NO_3^- concentrations decrease substantially across
371 most of the US but increase in Arizona, New Mexico and Mexico. When the VGLAI scheme is implemented,
372 concentrations of all species decrease by 2-10% throughout most of the domain, except for NO_3^- in the southwestern
373 U.S. and Mexico where predicted concentrations increase significantly (up to +51%).

374 Statistical evaluation of bulk PM_{10} , bulk $PM_{2.5}$, and $PM_{2.5}$ organic carbon (OC) concentrations with
375 combined measurement datasets show substantial improvement for bias metrics when the VGLAI scheme is used
376 (Table 6). CMAQ underpredicts PM_{10} across the three networks regardless of the particle dry deposition scheme
377 used, with mean biases of $-9.78 \mu\text{g m}^{-3}$ (PR11), $-6.03 \mu\text{g m}^{-3}$ (OFF), and $-6.56 \mu\text{g m}^{-3}$ (VGLAI). Compared with
378 PR11, both OFF and VGLAI reduce negative fractional biases by 46% and 41%, respectively, while the absolute
379 mean bias for each decrease by 3-4 $\mu\text{g m}^{-3}$. The fractional error for PM_{10} decreases by about 15%. For bulk $PM_{2.5}$,
380 CMAQ using the OFF scheme performs worse than with PR11, increasing all bias metrics modestly. However, with
381 the VGLAI scheme, mean and normalized mean biases are reduced by about half, with fractional bias reduced by 67%
382 compared to PR11. Fractional error is similar across all three cases. $PM_{2.5}$ OC performance for each case mirrors the
383 results of bulk $PM_{2.5}$, with mean bias reduced from $0.45 \mu\text{g m}^{-3}$ (PR11) to $0.39 \mu\text{g m}^{-3}$ (VGLAI). We note that while
384 Shu et al. (2017) found that CMAQv5.0.1 underestimated OC compared to ambient observations, CMAQv5.2.1 and
385 v5.3 (Appel et al., 2020) both predict OC well, with just a slight overprediction on average, the result of revised
386 organic aerosol formation and loss pathways incorporated in the CMAQ system between versions 5.0.1 and 5.2.1
387 (e.g. Pye and Pouliot, 2012; Pye et al., 2013; Pye et al., 2015; Murphy et al., 2017; Pye et al., 2017) and 5.3 (Xu et
388 al., 2018). Performance for inorganic $PM_{2.5}$ species is considerably more mixed (Table S4) with SO_4^{2-} , NO_3^- and
389 NH_4^+ biases increasing when VGLAI is implemented, and EC biases reduced slightly.

390 **5 Conclusions**

391 This study has documented the motivation, details, and impacts of incremental improvements to particle
392 dry deposition in CMAQv5.3, which has been updated with the VGLAI scheme. We have shown that the substantial
393 difference in fine particle V_d between CMAQv5.0.1 and CAMx v5.4.1 documented by Shu et al. (2017) are partly
394 attributable to the lack of consideration of polydispersity in the CAMx scheme, and partly to a numerically

395 unconstrained integration approach applied to the formulation of the impact efficiency in the PR11 scheme. We
396 update the conclusions of Shu et al. (2017) after finding that CMAQv5.2.1 does not underpredict $PM_{2.5}$ OC
397 compared to network observations, and that available particle dry V_d measurements indicate that both the CMAQ
398 and CAMx particle dry deposition schemes underpredict V_d in the fine particle regime, particularly for vegetative
399 surfaces. Updating these schemes in current CTMs, which presently show relatively good model performance for
400 fine particle predictions against routine network observations, will likely require additional upward revisions to
401 particle emission and formation rates. The most significant impact of the new CMAQ particle dry deposition scheme
402 was the enhancement of PM_{10} concentrations, which reduced negative biases of PM_{10} predictions by one third to one
403 half. More research is needed to constrain production and loss of coarse particles in atmospheric models, especially
404 natural resuspension processes like wind-blown dust and sea spray.

405 Our detailed analysis of the CMAQ particle dry deposition scheme highlights several key issues to keep in
406 mind for current application and future development. First, recently published empirical fits to available dry
407 deposition observations (e.g. Saylor et al., 2019; Emerson et al., 2020) are extremely promising and provide
408 encouraging performance improvements, especially for fine particle deposition. However, they still rely on
409 parameterization of unknown or physically abstract processes (i.e. interception) to describe the variability observed
410 in particle size and land-use type. Future dry deposition studies will hopefully lead to fully process-based
411 approaches so that theory may be more confidently extrapolated to environmental scenarios unconstrained by
412 measurements. Second, most studies, including this one, evaluate particle dry deposition schemes using field data,
413 simplifying or ignoring the uncertainty introduced by meteorological variability, uncertainty in characterizing
414 surface properties, and unknown source processes within complex systems, like vegetative canopies. Thus,
415 correction factors, like F_f in the PR11 scheme are not fully constrained. Future studies should evaluate performance
416 under varying convective conditions and consider the role of both formation and loss of particulate matter near the
417 surface (e.g., in forest canopies). Third, the application of particle dry deposition schemes to particle size
418 distributions in CTMs involves assumptions about how to project the process impacts to bulk variables, modes, or
419 sections. If a bulk approach is used, we recommend assuming a mode width and integrating the V_d using Eqs. 2 and
420 3 to avoid underestimating deposition of the particle population. For modal approaches, developers should be
421 mindful of the large impact mode standard deviation can have on the polydisperse V_d , depending on how size-
422 dependent deposition parameters are integrated. It may be prudent to fix this parameter to a mode-dependent
423 constant value in models as many large-scale CTMs already elect to do. Finally, contemporary particle dry
424 deposition measurement studies are often able to report size-dependent data. This is a crucial capability that reduces
425 uncertainty due to the polydispersity of the underlying particle population. It would be interesting to determine to
426 what extent historical bulk V_d observations are affected by assumptions of monodispersity or, in some cases, a
427 nominal mode width.

428 Comparing particle dry deposition schemes across large-scale CTMs is perhaps more challenging than
429 appreciated since the effect of mechanistic dry deposition schemes on model predictions can be difficult to
430 disentangle from uncertainties in other processes like resuspension and vertical mixing. We continue to need
431 integrated efforts that combine advanced field measurements, process-level insights, and large-scale atmospheric

432 models for better understanding the impact of particle dry deposition on broader environmental concerns like
433 climate change and human exposure to poor air quality.

434 **Data availability**

435 CMAQ source code, including updated particle dry deposition scheme (VGLAI), is freely available via
436 <http://github.com/usepa/cmaq.git>. Archived CMAQ versions including previous particle dry deposition scheme
437 (PR11) are available from the same repository. 0-D box model (Depoboxtoolv1.0) source code is freely available via
438 <https://github.com/shumarkq/Depoboxtool/tree/master>.

439 **Competing interests**

440 The authors declare that they have no conflict of interests.

441 **Disclaimer**

442 The views expressed in this article are those of the authors and do not necessarily represent the views or policies of
443 the U.S. Environmental Protection Agency.

444 **Acknowledgments**

445 This project was supported in part by an appointment to the Research Participation Program at the Office of
446 Research and Development, US Environmental Protection Agency, administered by the Oak Ridge Institute for
447 Science and Education through an interagency agreement between the US Department of Energy and the EPA.
448 Special thanks to Jonathan E. Pleim (EPA) for providing the idea and significant contributions to the development of
449 VGLAI scheme. Special thanks Rick D. Saylor (NOAA) for sharing literature field measurements data of dry
450 deposition velocities. Special thanks to Delphine K. Farmer and Ethan W. Emerson (CSU) for sharing literature
451 measurements.

452 **References**

453 Appel, K. W., Bash, J. O., Fahey, K. M., Foley, K. M., Gilliam, R. C., Hogrefe, C., Hutzell, W. T., Kang, D.,
454 Mathur, R., Murphy, B. N., Napelenok, S. L., Nolte, C. G., Pleim, J. E., Pouliot, G. A., Pye, H. O. T., Ran, L.,
455 Roselle, S. J., Sarwar, G., Schwede, D. B., Sidi, F. I., Spero, T. L. and Wong, D. C.: The Community Multiscale Air
456 Quality (CMAQ) Model Versions 5.3 and 5.3.1: System Updates and Evaluation, *Geosci. Model Dev. Discuss.*, 1–
457 41, <https://doi.org/10.5194/gmd-2020-345>, 2020.

458 Appel, K. W., Gilliam, R. C., Davis, N., Zubrow, A. and Howard, S. C.: Overview of the atmospheric model
459 evaluation tool (AMET) v1.1 for evaluating meteorological and air quality models, *Environ. Model. Softw.*, 26(4),
460 434–443, <https://doi.org/10.1016/j.envsoft.2010.09.007>, 2011.

461 Appel, K. W., Napelenok, S. L., Foley, K. M., Pye, H. O. T., Hogrefe, C., Luecken, D. J., Bash, J. O., Roselle, S. J.,
462 Pleim, J. E., Foroutan, H., Hutzell, W. T., Pouliot, G. A., Sarwar, G., Fahey, K. M., Gantt, B., Gilliam, R. C., Kang,
463 D., Mathur, R., Schwede, D. B., Spero, T. L., Wong, D. C., and Young, J. O.: Description and evaluation of the
464 Community Multiscale Air Quality (CMAQ) model version 5.1, *Geosci. Model Dev.*, 10, 1703-1732,
465 doi:10.5194/gmd-1703-2017, 2017.

466 Bash, J. O., Baker, K. R. and Beaver, M. R.: Evaluation of improved land use and canopy representation in BEIS
467 v3.61 with biogenic VOC measurements in California, *Geosci. Model Dev.*, 9(6), 2191–2207,
468 <https://doi.org/10.5194/gmd-9-2191-2016>, 2016.

469 Binkowski, F. S. and Shankar, U.: The Regional Particulate Matter Model: 1. Model description and preliminary
470 results, *J. Geophys. Res. Atmospheres*, 100(D12), 26191–26209, <https://doi.org/10.1029/95JD02093>, 1995.

471 Davidson, C. I., Miller, J. M. and Pleskow, M. A.: The influence of surface structure on predicted particle dry
472 deposition to natural grass canopies, *Water. Air. Soil Pollut.*, 18(1), 25–43, <https://doi.org/10.1007/BF02419401>,
473 1982.

474 Dyer, J. M.: Revisiting the Deciduous Forests of Eastern North America, *BioScience*, 56(4), 341–352,
475 [https://doi.org/10.1641/0006-3568\(2006\)56\[341:RTDFOE\]2.0.CO;2](https://doi.org/10.1641/0006-3568(2006)56[341:RTDFOE]2.0.CO;2), 2006.

476 Emerson, E. W., Hodshire, A. L., DeBolt, H. M., Bilsback, K. R., Pierce, J. R., McMeeking, G. R. and Farmer, D.
477 K.: Revisiting particle dry deposition and its role in radiative effect estimates, *Proc. Natl. Acad. Sci.*, 117(42),
478 26076–26082, <https://doi.org/10.1073/pnas.2014761117>, 2020.

479 Foroutan, H., Young, J., Napelenok, S., Ran, L., Appel, K. W., and Pleim, J. E.: Development and evaluation of a
480 physics-based windblown dust emission scheme in the CMAQ modeling system, *J. Adv. Model. Earth Sy.*, 9,
481 doi:10.1002/2016MS000823, 2017.

482 Giorgi, F., 1986. A particle dry-deposition parameterization scheme for use in tracer transport models. *J. Geophys.*
483 *Res. Atmospheres* 91, 9794–9806. <https://doi.org/10.1029/JD091iD09p09794>

484 Giorgi, F.: Dry deposition velocities of atmospheric aerosols as inferred by applying a particle dry deposition
485 parameterization to a general circulation model, *Tellus B Chem. Phys. Meteorol.*, 40(1), 23–41,
486 <https://doi.org/10.3402/tellusb.v40i1.15627>, 1988.

487 Henderson, B. H., Akhtar, F., Pye, H. O. T., Napelenok, S. L. and Hutzell, W. T.: A database and tool for boundary
488 conditions for regional air quality modeling: description and evaluation, *Geosci. Model Dev.*, 7(1), 339–360,
489 <https://doi.org/10.5194/gmd-7-339-2014>, 2014.

490 Kang, D., Pickering, K. E., Allen, D. J., Foley, K. M., Wong, D. C., Mathur, R. and Roselle, S. J.: Simulating
491 lightning NO production in CMAQv5.2: evolution of scientific updates, *Geosci. Model Dev.*, 12(7), 3071–3083,
492 <https://doi.org/10.5194/gmd-12-3071-2019>, 2019.

493 Khan, T. R. and Perlinger, J. A.: Evaluation of five dry particle deposition parameterizations for incorporation into
494 atmospheric transport models, *Geosci. Model Dev.*, 10(10), 3861–3888, <https://doi.org/10.5194/gmd-10-3861-2017>,
495 2017.

496 Lamaud, E., Brunet, Y., Labatut, A., Lopez, A., Fontan, J. and Druilhet, A.: The Landes experiment: Biosphere-
497 atmosphere exchanges of ozone and aerosol particles above a pine forest, *J. Geophys. Res. Atmospheres*, 99(D8),
498 16511–16521, <https://doi.org/10.1029/94JD00668>, 1994.

499 Lovett, G. M.: Atmospheric Deposition of Nutrients and Pollutants in North America: An Ecological Perspective,
500 *Ecol. Appl.*, 4(4), 629–650, <https://doi.org/10.2307/1941997>, 1994.

501 Matsuda, K., Fujimura, Y., Hayashi, K., Takahashi, A. and Nakaya, K.: Deposition velocity of PM_{2.5} sulfate in the
502 summer above a deciduous forest in central Japan, *Atmos. Environ.*, 44(36), 4582–4587,
503 <https://doi.org/10.1016/j.atmosenv.2010.08.015>, 2010.

504 Murphy, B.N., Woody, M.C., Jimenez, J.L., Carlton, A.M.G., Hayes, P.L., Liu, S., Ng, N.L., Russell, L.M., Setyan,
505 A., Xu, L. and Young, J., 2017. Semivolatile POA and parameterized total combustion SOA in CMAQv5. 2:
506 impacts on source strength and partitioning. *Atmospheric chemistry and physics*, 17(18), pp.11107-11133.

507 Nemitz, E., Gallagher, M. W., Duyzer, J. H. and Fowler, D.: Micrometeorological measurements of particle
508 deposition velocities to moorland vegetation, *Q. J. R. Meteorol. Soc.*, 128(585), 2281–2300,
509 <https://doi.org/10.1256/qj.01.71>, n.d.

510 Nolte, C. G., Appel, K. W., Kelly, J. T., Bhave, P. V., Fahey, K. M., Collett Jr., J. L., Zhang, L. and Young, J. O.:
511 Evaluation of the Community Multiscale Air Quality (CMAQ) model v5.0 against size-resolved measurements of
512 inorganic particle composition across sites in North America, *Geosci. Model Dev.*, 8(9), 2877–2892,
513 <https://doi.org/10.5194/gmd-8-2877-2015>, 2015.

514 Peters, K. and Eiden, R.: Modelling the dry deposition velocity of aerosol particles to a spruce forest, *Atmospheric*
515 *Environ. Part Gen. Top.*, 26(14), 2555–2564, [https://doi.org/10.1016/0960-1686\(92\)90108-W](https://doi.org/10.1016/0960-1686(92)90108-W), 1992.

516 Petroff, A., Mailliat, A., Amielh, M. and Anselmet, F.: Aerosol dry deposition on vegetative canopies. Part I:
517 Review of present knowledge, *Atmos. Environ.*, 42(16), 3625–3653,
518 <https://doi.org/10.1016/j.atmosenv.2007.09.043>, 2008.

519 Pleim, J. and Ran, L.: Surface Flux Modeling for Air Quality Applications, *Atmosphere*, 2(3), 271–302,
520 <https://doi.org/10.3390/atmos2030271>, 2011.

521 Pryor, S. C., Gallagher, M., Sievering, H., Larsen, S. E., Barthelmie, R. J., Birsan, F., Nemitz, E., Rinne, J.,
522 Kulmala, M., Grönholm, T., Taipale, R. and Vesala, T.: A review of measurement and modelling results of particle
523 atmosphere–surface exchange, *Tellus B Chem. Phys. Meteorol.*, 60(1), 42–75, <https://doi.org/10.1111/j.1600-0889.2007.00298.x>, 2008.

525 Pye, H.O. and Pouliot, G.A., 2012. Modeling the role of alkanes, polycyclic aromatic hydrocarbons, and their
526 oligomers in secondary organic aerosol formation. *Environmental science & technology*, 46(11), pp.6041-6047.
527

528 Pye, H.O., Pinder, R.W., Piletic, I.R., Xie, Y., Capps, S.L., Lin, Y.H., Surratt, J.D., Zhang, Z., Gold, A., Luecken,
529 D.J. and Hutzell, W.T., 2013. Epoxide pathways improve model predictions of isoprene markers and reveal key role
530 of acidity in aerosol formation. *Environmental science & technology*, 47(19), pp.11056-11064.
531

532 Pye, H.O., Murphy, B.N., Xu, L., Ng, N.L., Carlton, A.G., Guo, H., Weber, R., Vasilakos, P., Appel, K.W.,
533 Budisulistiorini, S.H. and Surratt, J.D., 2017. On the implications of aerosol liquid water and phase separation for
534 organic aerosol mass. *Atmospheric chemistry and physics*, 17(1), pp.343-369.

535 Riemer, N., Ault, A. P., West, M., Craig, R. L. and Curtis, J. H.: Aerosol Mixing State: Measurements, Modeling,
536 and Impacts, *Rev. Geophys.*, 57(2), 187–249, <https://doi.org/10.1029/2018RG000615>, 2019.

537 Ruijrok, W., Davidson, C. I. and Nicholson, K. W.: Dry deposition of particles, *Tellus B*, 47(5), 587–601,
538 <https://doi.org/10.1034/j.1600-0889.47.issue5.6.x>, 1995.

539 Saylor, R. D., Baker, B. D., Lee, P., Tong, D., Pan, L. and Hicks, B. B.: The particle dry deposition component of
540 total deposition from air quality models: right, wrong or uncertain?, *Tellus B Chem. Phys. Meteorol.*, 71(1),
541 1550324, <https://doi.org/10.1080/16000889.2018.1550324>, 2019.

542 Shu, Q., Koo, B., Yarwood, G. and Henderson, B. H.: Strong influence of deposition and vertical mixing on
543 secondary organic aerosol concentrations in CMAQ and CAMx, *Atmos. Environ.*, 171(Supplement C), 317–329,
544 <https://doi.org/10.1016/j.atmosenv.2017.10.035>, 2017.

545 Slinn, S. A. and Slinn, W. G. N.: Predictions for particle deposition on natural waters, *Atmospheric Environ.* 1967,
546 14(9), 1013–1016, [https://doi.org/10.1016/0004-6981\(80\)90032-3](https://doi.org/10.1016/0004-6981(80)90032-3), 1980.

547 Slinn, W. G. N.: Precipitation chemistry Predictions for particle deposition to vegetative canopies, *Atmospheric*
548 *Environ.* 1967, 16(7), 1785–1794, [https://doi.org/10.1016/0004-6981\(82\)90271-2](https://doi.org/10.1016/0004-6981(82)90271-2), 1982.

549 Venkatram, A.: Estimating the convective velocity scale for diffusion applications, *Bound.-Layer Meteorol.*, 15(4),
550 447–452, <https://doi.org/10.1007/BF00120606>, 1978.

551 Venkatram, A. and Pleim, J.: The electrical analogy does not apply to modeling dry deposition of particles, *Atmos.*
552 *Environ.*, 33(18), 3075–3076, [https://doi.org/10.1016/S1352-2310\(99\)00094-1](https://doi.org/10.1016/S1352-2310(99)00094-1), 1999.

553 Vong, R. J., Vickers, D. and Covert, D. S.: Eddy correlation measurements of aerosol deposition to grass, *Tellus B*,
554 56(2), 105–117, <https://doi.org/10.1111/j.1600-0889.2004.00098.x>, 2004.

555 Wesely, M. L. and Hicks, B. B.: Some Factors that Affect the Deposition Rates of Sulfur Dioxide and Similar Gases
556 on Vegetation, *J. Air Pollut. Control Assoc.*, 27(11), 1110–1116, <https://doi.org/10.1080/00022470.1977.10470534>,
557 1977.

558 Wiman, B. L. B. and Ågren, G. I.: Aerosol depletion and deposition in forests—A model analysis, *Atmospheric*
559 *Environ.* 1967, 19(2), 335–347, [https://doi.org/10.1016/0004-6981\(85\)90101-5](https://doi.org/10.1016/0004-6981(85)90101-5), 1985.

560 Xiu, A. and Pleim, J. E.: Development of a Land Surface Model. Part I: Application in a Mesoscale Meteorological
561 Model, *J. Appl. Meteorol.*, 40(2), 192–209, [https://doi.org/10.1175/1520-0450\(2001\)040<0192:DOALSM>2.0.CO;2](https://doi.org/10.1175/1520-0450(2001)040<0192:DOALSM>2.0.CO;2), 2001.

563 Xu, Lu, et al. "Experimental and model estimates of the contributions from biogenic monoterpenes and
564 sesquiterpenes to secondary organic aerosol in the southeastern United States." *Atmospheric chemistry and*
565 *physics* 18.17 (2018): 12613-12637.
566

567 Zhang, L., Gong, S., Padro, J. and Barrie, L.: A size-segregated particle dry deposition scheme for an atmospheric
568 aerosol module, *Atmos. Environ.*, 35(3), 549–560, [https://doi.org/10.1016/S1352-2310\(00\)00326-5](https://doi.org/10.1016/S1352-2310(00)00326-5), 2001.

569

Table 1. Detailed mechanistic expressions used for particle dry deposition velocity and resistance parameters for monodisperse and sectional approaches.

Scheme	V_d	R_a	R_s
PR11 ^a	$\frac{V_g}{1 - e^{-V_g(R_a+R_s)}}$	$\phi_{hn} \frac{\ln\left(\frac{Z_R}{Z_0}\right) - \Psi_H}{\kappa u_*}$	$\frac{1}{F_f u_* E_{Tot}}$
OFF ^b	$\frac{V_g}{1 - e^{-V_g(R_a+R_s)}}$	$\phi_{hn} \frac{\ln\left(\frac{Z_R}{Z_0}\right) - \Psi_H}{\kappa u_*}$	$\frac{1}{F_f u_* E_{Tot}}$
VGLAI ^c	$\frac{V_g}{1 - e^{-V_g(R_a+R_s)}}$	$\phi_{hn} \frac{\ln\left(\frac{Z_R}{Z_0}\right) - \Psi_H}{\kappa u_*}$	$\frac{1}{\left(1 + f_{veg}(\max(LAI - 1, 0))\right) F_f u_* E_{Tot}}$
Z01 ^d	$V_g + \frac{1}{R_a + R_s}$	$\phi_{hn} \frac{\ln\left(\frac{Z_R}{Z_0}\right) - \Psi_H}{\kappa u_*}$	$\frac{1}{\varepsilon_0 u_* E_{Tot} R_1}$

V_g = settling velocity: $V_g = \frac{\rho d_p^2 g C}{18\mu}$ (m s⁻¹)

ρ = particle density (kg m⁻³)

d_p = particle diameter (m)

g = acceleration due to gravity (m s⁻²)

C = Cunningham slip-correction factor: $C = 1 + \frac{2\lambda}{d_p} (1.257 + 0.4e^{-\frac{0.55d_p}{\lambda}})$

μ = temperature-dependent viscosity of air (kg m⁻¹ s⁻¹)

λ = the mean free path of air (m)

ϕ_{hn} = non-dimensional temperature profile constant for neutral conditions

Z_R = height at which dry deposition velocity is measured (m)

Z_0 = roughness length (m)

Ψ_H = stability correction function for heat (see an example expression in Khan and Perlinger, 2017)

κ = Von Karman constant

u_* = friction velocity (m s⁻¹)

E_{Tot} = Total of all deposition process efficiencies: $E_{Tot} = E_B + E_{IM} + E_{IN}$ (see detailed expressions for

E_B, E_{IM}, E_{IN} in Table 2)

E_B = Brownian diffusion efficiency

E_{IM} = Impaction efficiency

E_{IN} = Interception F_f = correction factor for convective conditions: $F_f = 1 + 0.24 \frac{w_*^2}{u_*^2}$

w_* = convective velocity scale (m s⁻¹)

ε_0 = empirical constant assumed to be 3 across all land-use types (Zhang et al., 2001)

R_1 = correction factor for fraction of particles that stick to the surface

^aBase CMAQ scheme (v4.5 to v5.2.1)

^bProposed CMAQ scheme (only tested in CMAQ v5.2.1 in this work)

^cProposed CMAQ scheme (tested in CMAQ v5.2.1 in this work and incorporated in CMAQ v5.3)

^dCAMx v5.4.1 and later

Table 2. Detailed mechanistic expressions used for particle dry deposition velocity, settling velocity and resistance parameters for monodisperse and sectional approaches.

Scheme	E_B	E_{IM}	E_{IN}	St	E_{IN}	St
				Smooth Surfaces	Vegetative Surfaces	
PR11^a	$Sc^{-\frac{2}{3}}$	$\frac{St^2}{400 + St^2}$	Assume 0	$\frac{V_g u_*^2}{g\nu}$	Assume 0	$\frac{V_g u_*^2}{g\nu}$
OFF^b	$Sc^{-\frac{2}{3}}$	$\frac{St^2}{400 + St^2}$	Assume 0	$\frac{V_g u_*^2}{g\nu}$	Assume 0	$\frac{V_g u_*^2}{g\nu}$
VGLAI^c	$Sc^{-\frac{2}{3}}$	$\frac{St^2}{1 + St^2}$	Assume 0	$\frac{V_g u_*}{gA}$	Assume 0	$\frac{V_g u_*}{gA}$
Z01^d	$Sc^{-\gamma}$	$\left(\frac{St}{\alpha + St}\right)^2$	Assume 0	$\frac{V_g u_*^2}{g\nu}$	$\frac{1}{2} \left(\frac{d_p}{A}\right)^2$	$\frac{V_g u_*}{gA}$

γ = empirical parameter dependent on land-use type. Ranges from 0.5 to 0.58

α = empirical parameter dependent on land-use type. Ranges from 0.8 to 100, but typically 1.0 or 1.2

ν = kinematic viscosity of air ($m^2 s^{-1}$)

A = characteristic radius of collectors on vegetative surfaces (m)

^{a, b, c, d}Same as Table 1.

Table 3. Modifications to particle dry deposition schemes for integrated modal forms.

Scheme	Integrated		
	Parameters for V_d Calculation	$\widehat{E}_{IM,k}$	\widehat{St}_k
PR11 ^a	$\widehat{D}_k, \widehat{V}_{g,k}, \widehat{E}_{IM,k}$	$\left(\frac{St^2}{400}\right) e^{(4k+8) \ln^2 \sigma_g}$	$\frac{V_g u_*^2}{g\nu}$
OFF ^b	$\widehat{D}_k, \widehat{V}_{g,k}$	$\frac{St^2}{400 + St^2}$	$\frac{V_g u_*^2}{g\nu}$
VGLAI ^c	$\widehat{D}_k, \widehat{V}_{g,k}, \widehat{St}_k, \widehat{E}_{IM,k}$	$\frac{\widehat{St}^2}{1 + \widehat{St}^2}$	$\frac{\widehat{V}_g u_*}{gA}$

k corresponds to the moment of the modal distribution being calculated (i.e., number = 0, surface area = 2, volume = 3).

^{a, b, c}Same as Table 1.

Table 4. Statistical evaluation of particle dry deposition schemes implemented in the box model for polydisperse particle populations across four land-use types.

Land-Use Type	Scheme ^a	Fractional Bias (FB) ^b	Fractional Error (FE) ^c	dR ²
Grass	PR11	-70.88	114.54	0.71
	OFF	-70.94	114.59	0.71
	VGLAI	-7.73	96.99	0.71
Coniferous Forest	PR11	-98.03	115.18	0.59
	OFF	-98.39	115.06	0.59
	VGLAI	-2.67	89.67	0.57
Deciduous Forest	PR11	-149.38	149.72	0.05
	OFF	-149.38	149.72	0.05
	VGLAI	-66.31	106.58	0.05
Water	PR11	-47.23	132.07	0.57
	OFF	-47.23	132.07	0.57
	VGLAI	-47.19	132.04	0.57

^a Modal standard deviation (σ_g) is assumed to be 1.01.

^b Fractional bias: $FB = \frac{2}{N} \sum \frac{M_i - O_i}{M_i + O_i}$, FB ranges from negative infinity to positive infinity with 0 indicating unbiased data.

^c Fractional error: $FE = \frac{2}{N} \sum \frac{|M_i - O_i|}{M_i + O_i}$, FE ranges from 0 (perfect performance) to positive infinity.

^d Coefficient of determination: $R^2 = \left\{ \frac{\sum(O_i - \bar{O})(M_i - \bar{M})}{\sqrt{\sum(O_i - \bar{O})^2 \sum(M_i - \bar{M})^2}} \right\}^2$, R² ranges from 0 to 1.

^f FB and FE are multiplied by 100.

Table 5. CMAQ deposition model performance for 2011 across CASTNET network.

Deposition Metric	Dry Deposition Scheme	Number of Observations	Mean Bias (MB) ^a	Normalized Mean Bias (NMB) ^b	Fractional Bias (FB) ^c	Fractional Error (FE) ^d	R ²
SO ₄ ²⁻	PR11	3992	-0.0083	-59.39	-84.23	94.24	0.32
	OFF		-0.0109	-78.21	-113.92	117.47	0.64
	VGLAI		-0.0071	-51.29	-65.47	76.27	0.59
NO ₃ ⁻	PR11	3992	-0.0031	-65.80	-85.55	110.70	0.20
	OFF		-0.0036	-76.41	-110.87	123.66	0.35
	VGLAI		-0.0031	-64.33	-73.89	101.68	0.25
NH ₄ ⁺	PR11	3992	0.0002	4.64	120.31	75.88	0.01
	OFF		-0.0011	-21.37	204.66	-18.95	0.01
	VGLAI		0.0007	13.41	105.03	94.4	0.01

^a Mean bias: $MB = \frac{1}{N} \sum M_i - O_i$, MB ranges from negative infinity to positive infinity with 0 indicating unbiased data.

^b Normalized mean bias: $NMB = \frac{1}{N} \sum \frac{M_i - O_i}{O_i}$, ranges from negative 1 to positive infinity with 0 indicating unbiased data.

^c Defined in Table 4.

^d Defined in Table 4.

^f MB unit is kg ha⁻¹.

^g NMB, FB and FE are multiplied by 100.

Table 6. CMAQ concentration model performance for 2011 with combined measurement datasets (AQS, CSN and IMPROVE).

Concentration Metric	Dry Deposition Scheme	Number of Observations	Mean Bias (MB) ^a	Normalized Mean Bias (NMB) ^b	Fractional Bias (FB) ^c	Fractional Error (FE) ^d	R ²
PM ₁₀ ^e	PR11	165312	-9.78	-45.09	-50.06	68.16	0.03
	OFF		-6.03	-27.77	-26.86	57.59	0.05
	VGLAI		-6.56	-30.25	-29.58	58.59	0.05
PM _{2.5}	PR11	473606	0.69	7.00	1.86	41.92	0.39
	OFF		0.73	7.46	2.73	41.73	0.39
	VGLAI		0.47	4.77	0.60	41.55	0.38
OC ^f	PR11	68428	0.45	29.84	15.00	55.22	0.29
	OFF		0.46	30.67	15.63	55.41	0.29
	VGLAI		0.39	25.97	12.79	54.63	0.29

^{a, b, c, d} Defined in Table 5.

^e Only AQS data.

^f PM_{2.5} organic carbon.

^g MB unit is µg m⁻³.

^h NMB, FB and FE are multiplied by 100.

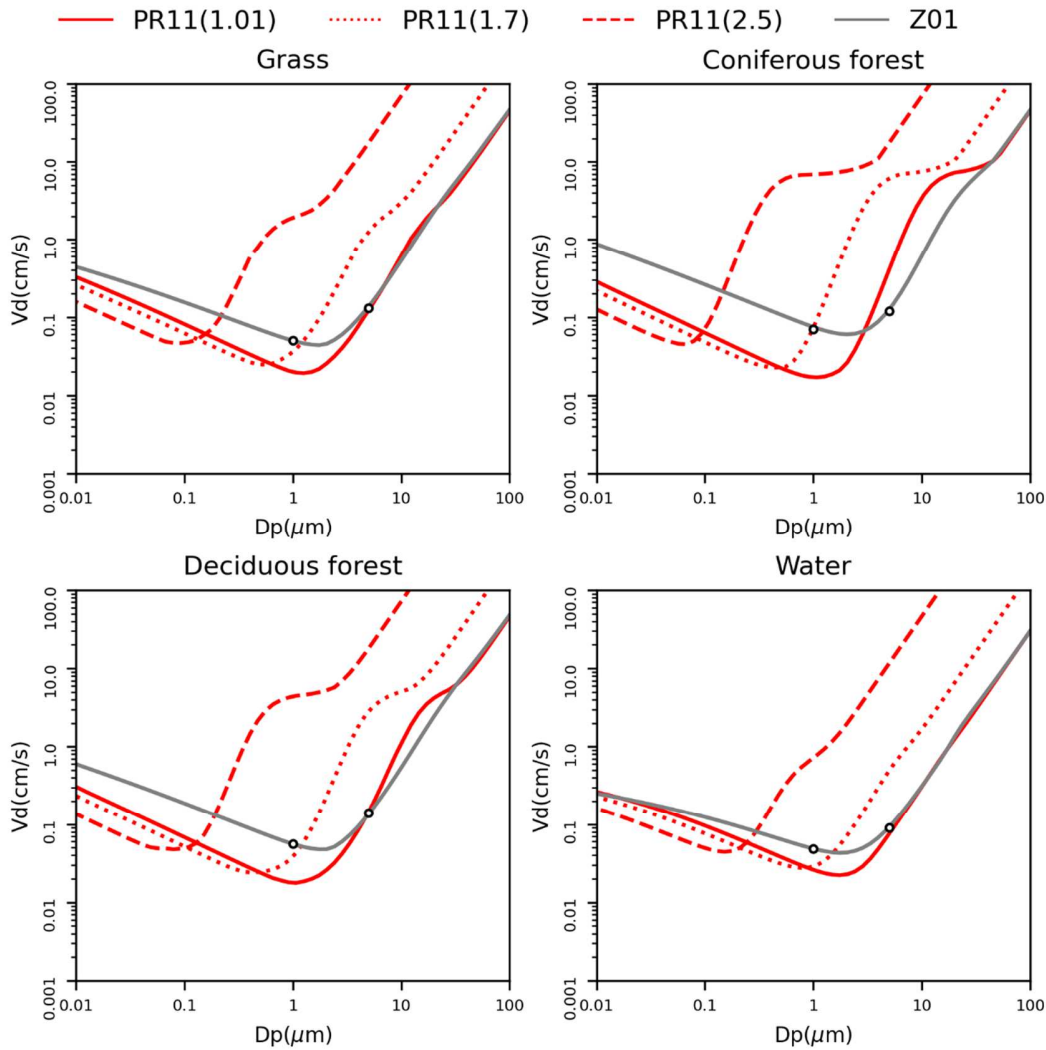


Figure 1. Comparison of CMAQ (PR11) and CAMx (Z01) particle dry deposition (V_d) schemes implemented in a box model as a function of monodisperse particle size for four land-use types. For the PR11 scheme, the trends are integrated for the deposition of the third moment of the modal particle size distribution with the x-axis corresponding to the geometric mean particle diameter of the mode. Each PR11 trend corresponds to a different value of σ_g which is denoted in parentheses, the modal standard deviation. For the Z01 scheme, the trend shown is for monodisperse particles, consistent with how the scheme is typically applied in the CAMx model. The black circle symbols identify the assumed sizes of particles in the CAMx coarse-fine approach. No full CAMx simulations were performed for this work.

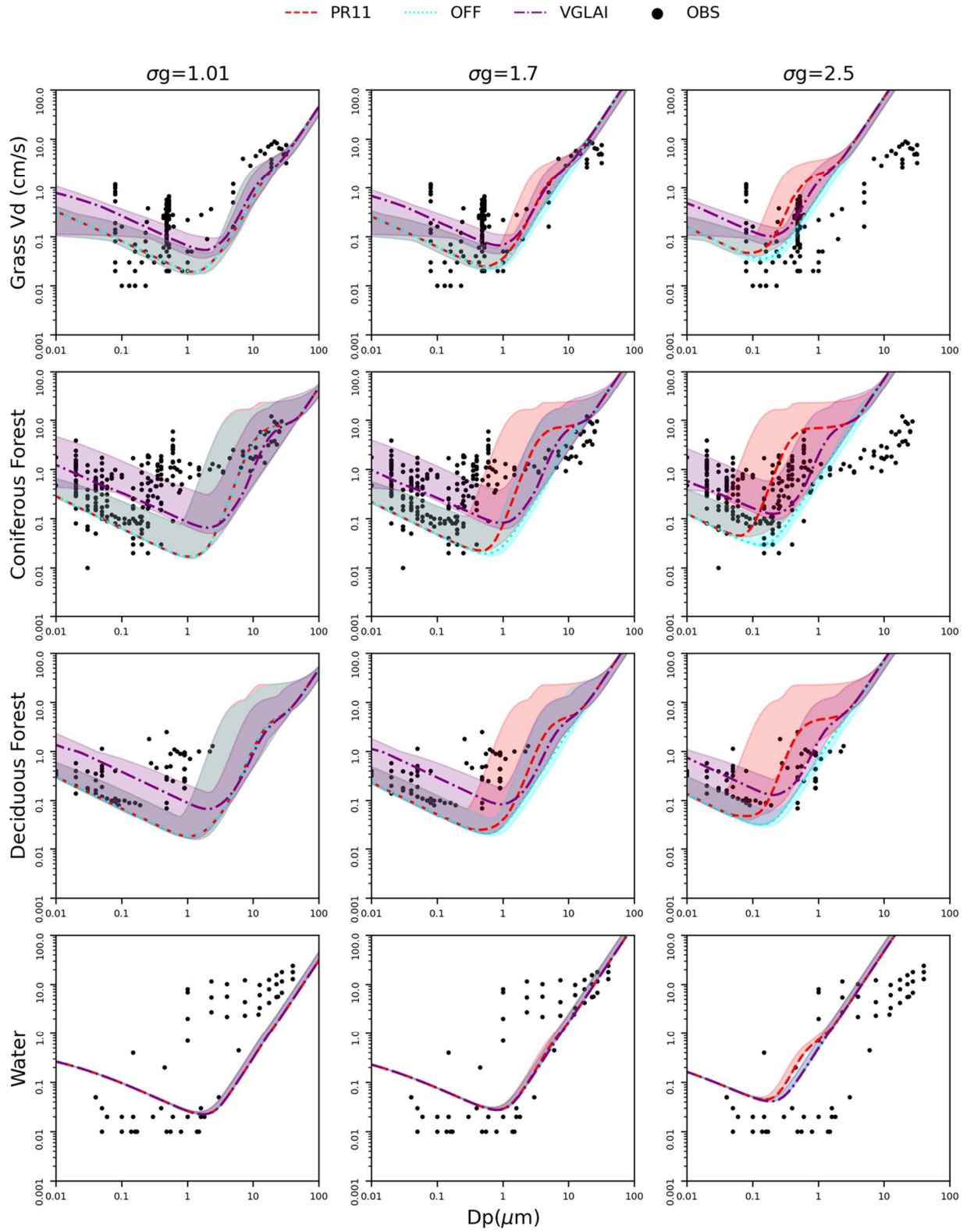


Figure 2. Particle dry V_d for the base PR11 scheme and two updated schemes (OFF and VGLAI) implemented in the box model as a function of polydisperse particle geometric mean diameter for four land-use types and three assumptions for modal standard deviation ($\sigma_g = 1.01, 1.7$ and 2.5). The trends correspond to the modal integrated V_d of the 3rd moment (i.e., particle volume). Details of the observations (black dots) are provided in the supporting information (Table S2).

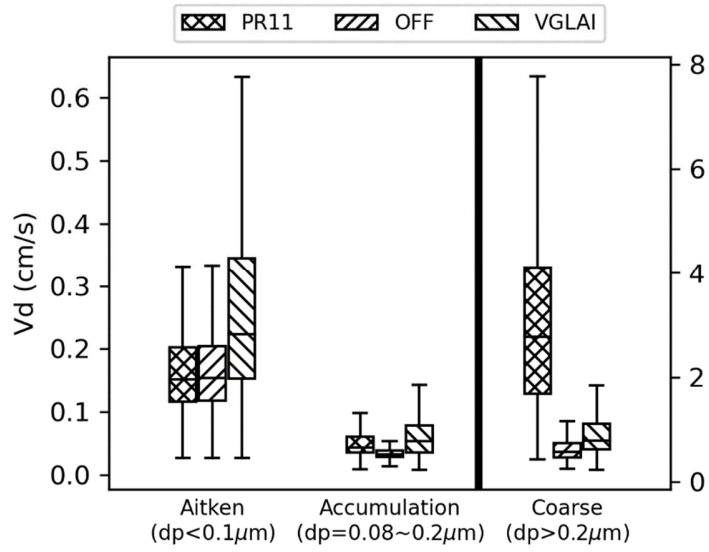


Figure 3. Annually averaged dry V_d predicted by CMAQv5.2.1 for the Aitken, accumulation, and coarse particle modes using the PR11, OFF, and VGLAI particle dry deposition schemes. The variability illustrated by the boxes and whiskers corresponds to spatial variability in annually averaged values throughout the CMAQ domain.

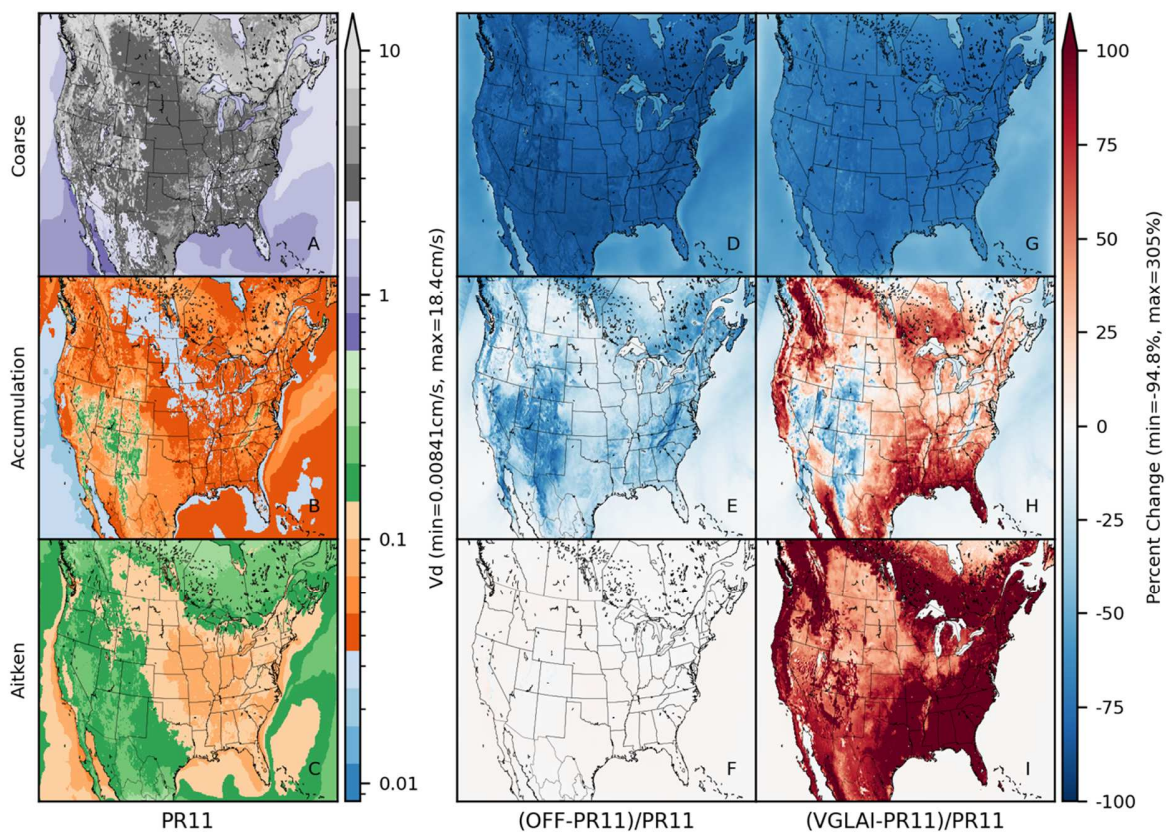
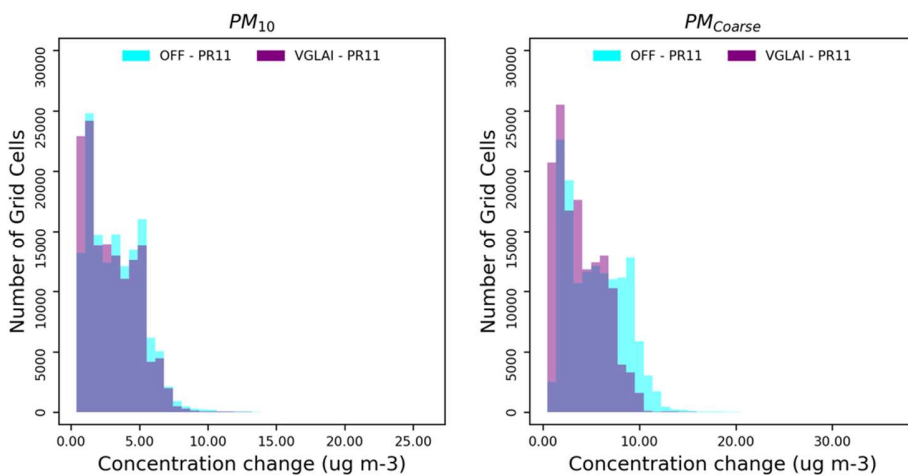


Figure 4. CMAQ estimated annual mean particle dry deposition velocity (cm/s) using PR11 for the Coarse, accumulation, and Aitken size modes (A, B, C) and the corresponding percent changes with updated dry deposition schemes for OFF (D, E, F) and VGLAI (G, H, I).

5



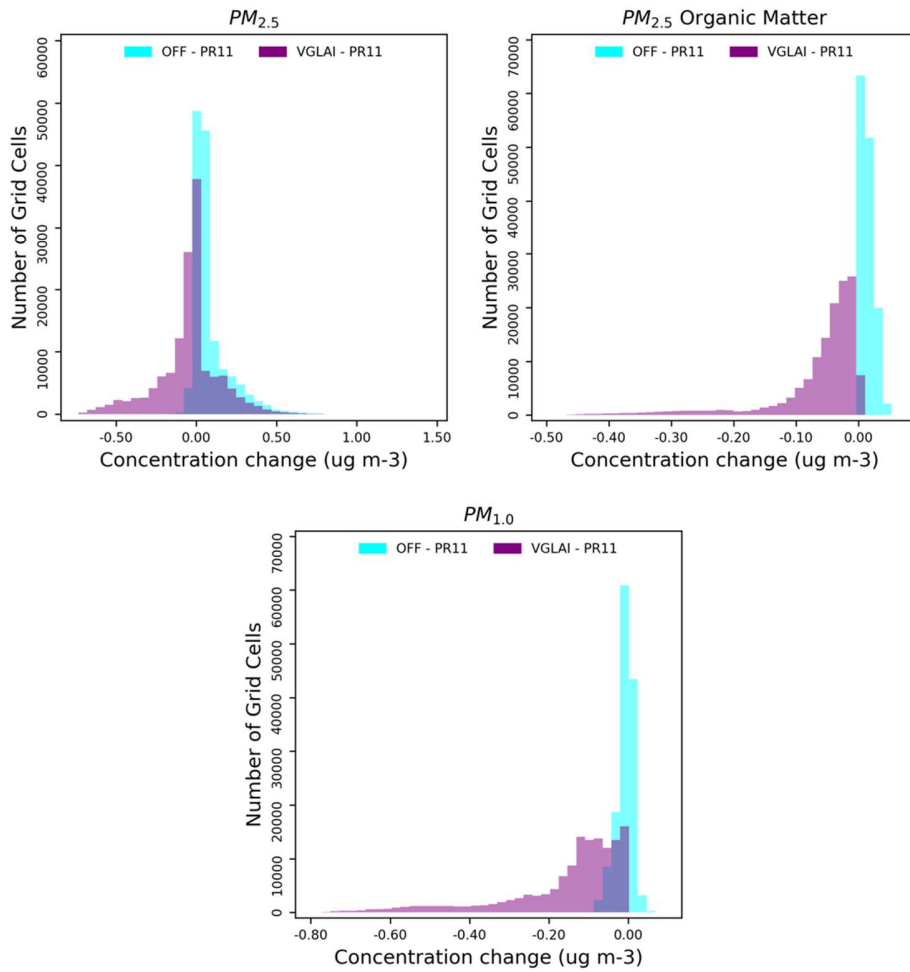


Figure 5. Histograms of the change in annually averaged concentration estimated by CMAQ for aggregate PM mass metrics between PR11 and the OFF and VGLAI particle dry deposition schemes. The variability illustrated by the histograms corresponds to spatial variability in annually averaged values throughout the CMAQ domain.

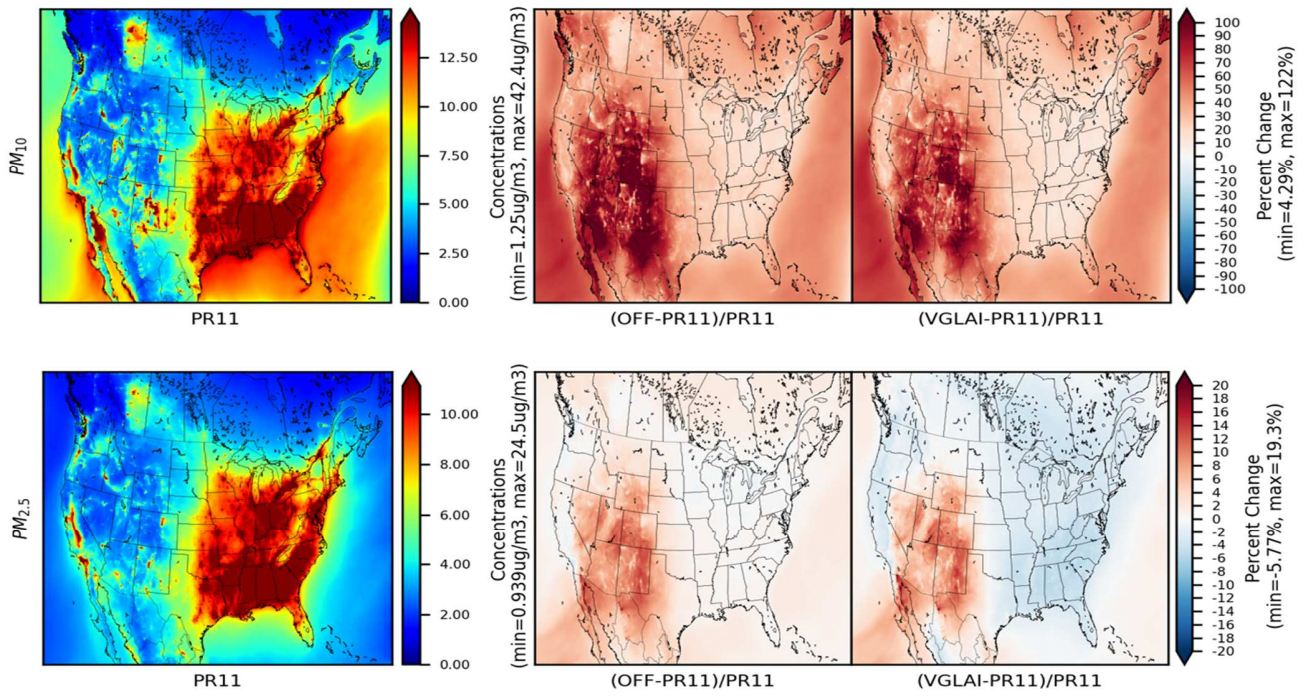


Figure 6. CMAQ estimated 2011 annual mean PM_{10} and $PM_{2.5}$ ($\mu g m^{-3}$) for the PR11 dry deposition scheme and the corresponding percent change using the OFF and VGLAI schemes.